Geomechanics and Engineering, *Vol. 30, No. 3 (2022) 219-231*
https://doi.org/10.12989/gae.2022.30.3.219

Effect of degree of compaction & confining stress on instability behavior of unsaturated soil

Ali Murtaza Rasool*[1,2,3,4]

[1]*National Engineering Services Pakistan (NESPAK), Lahore, Pakistan*
[2]*University of Central Punjab (UCP), Lahore, Pakistan*
[3]*National College of Arts (NCA), Lahore, Pakistan*
[4]*Department of Civil & Environmental Engineering, Saitama University, Japan*

(*Received August 3, 2020, Revised February 15, 2022, Accepted June 6, 2022*)

Abstract. Geotechnical materials such as silt, fine sand, or coarse granular soils may be unstable under undrained shearing or during rainfall infiltration starting an unsaturated state. Some researches are available describing the instability of coarse granular soils in drained or undrained conditions. However, there is a need to investigate the instability mechanism of unsaturated silty soil considering the effect of degree of compaction and net confining stress under partially and fully drained conditions. The specimens in the current study are compacted at 65%, 75%, & 85% degree of compaction, confined at pressures of 60, 80 & 120 kPa, and tested in partially and fully drained conditions. The tests have been performed in two steps. In Step-I, the specimens were sheared in constant water content conditions (a type of partially drained test) to the maximum shear stress. In Step-II, shearing was carried in constant suction conditions (a type of fully undrained test) by keeping shear stress constant. At the start of Step-II, PWP was increased in steps to decrease matric suction (which was then kept constant) and start water infiltration. The test results showed that soil instability is affected much by variation in the degree of compaction and confining stresses. It is also observed that loose and medium dense soils are vulnerable to pre-failure instability i.e., instability occurs before reaching the failure state, whereas, instability in dense soils instigates together with the failure i.e., failure line (FL) and instability line (IL) are found to be unique.

Keywords: constant shear stress; degree of compaction; failure line; instability; water infiltration

1. Introduction

Most of the embankments, natural slopes, and artificial soil structures are made of compacted soils. Infiltration in the soil is an important phenomena and its effect on stability is studied by Liu *et al*. (2017), Qi *et al*. (2019), Song and Hong (2020). Both drained and undrained shear strength of compacted soils is of significance in dealing with such structures. It is said that the failure of these structures can be initiated by the instability of soil. Instability is defined as the behavior of soil in which large plastic strains are produced to withstand stress i.e., shearing (Chu *et al*. 2003, Zhao and Zhang 2014). Generally, it is considered that if the stress state of a soil element satisfied the failure criterion, instability is said to have occurred. The conventional stability analysis is also performed on assumption that the instability will not occur unless the stress state of soil reaches the Mohr-Coulomb failure/plastic limit criterion. The Mohr-Coulomb failure criterion is commonly used to describe the strength of soils, whereas, the extended Mohr-Coulomb failure criteria (Fredlund *et al*. 2012) defines the shear strength of unsaturated soil. Mohr-Coulomb criteria is used by many researchers to define the behavior of soils (Chen *et al.* 2013, Consoli *et al.* 2015, Labuz and Zang 2012, Rahardjo *et al.* 2019, Rasool and Kuwano 2018). Recent theoretical development and experimental investigations indicated that instability is initiated once the loose soil reaches peak undrained shear strength (Andrade *et al.* 2013, Lashkari 2016, Rasool *et al.* 2020, Sun 2013). However, instability may also occur before attaining the failure stress state. When it occurs before attaining failure state is termed as prefailure instability and observed mainly for saturated loose sand under drained conditions (Chu and Wanatowski 2009, Leong *et al.* 2000). Static liquefaction is an example that occurs before the effective stress path reaches the failure line (Chu *et al.* 2011). Desai *et al.* (2005), Rahman *et al.* (2014) have developed various constitutive models, whereas, some experimental studies have been performed by Gajo *et al*. (2000), Chu *et al*. (2003), Daouadji *et al*. (2010) to predict the occurrence of instability before failure line (*FL*). Generally, shear stress is kept constant in tests to determine the instability, however, the review of previous studies showed that due to limitation of triaxial loading system it is difficult to maintain shear stress during the test and its variation significantly affects the determination of instability (Monkul *et al.* 2011). The most important factor affecting the instability is the shear stress level at which it is maintained constant (Dong *et al.* 2016, Rasool and Kuwano 2020c). Many researchers have used drained laboratory experiments to examine the instability behavior of granular

*Corresponding author, Senior Engineer
E-mail: ali.murtaza@nespak.com.pk,
ali_eng@hotmail.com

ISSN: 2005-307X (Print), 2092-6219 (Online)

Table 1 Composition and physical properties of DL clay

Soil Composition		
Silt	%	90.5
Clay	%	9.5
Physical properties of soil		
Soil particle density, ρ_s	g/cm^3	2.65
Consistency	-	NP
Maximum particle size, d_{max}	mm	0.039

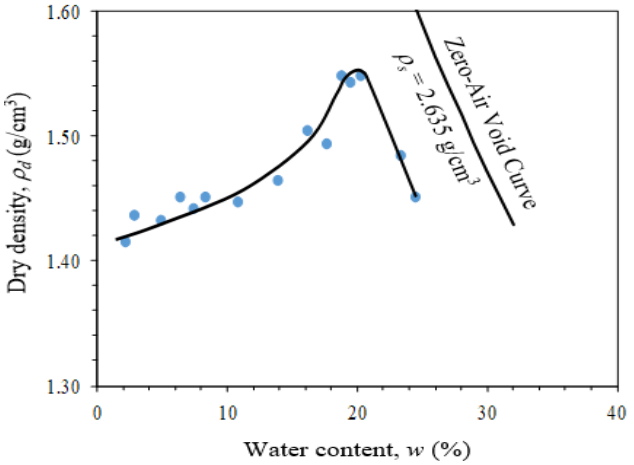

Fig. 1 Compaction characteristics of DL clay

materials, the tests were performed by keeping the shear strength constant at 80-90% of maximum shear strength and infiltrating the water in the soil (Gui and Wu 2014, Meilani *et al.* 2005, Melinda *et al.* 2004, Rasool and Kuwano 2020a). The results of these studies were limited and could not give much information on how the instability is affected when the stress state of the specimen is changed due to a change in compaction effort or confining stress. Therefore, there is a need to investigate the instability of unsaturated soil considering the effect of the degree of compaction and confining stress under partially and fully drained conditions. Given above, an experimental program is designed to investigate the effect of degree on compaction and confining stresses on the instability of unsaturated soil under partially and fully drained conditions. The instability is measured in terms of change in pore water pressure, degree of saturation, volumetric strain, and shear stress when subjected to drained stress path. Besides, the effect of instability on stress path and failure line (*FL*) is also studied and discussed.

2. Tested soil

As per the USCS classification system (ASTM D2487-17, 2017), the soil used in this study is categorized as silt with 90.5% silt and 9.5% clay contents. Its optimum water content (*OMC*) is 20% and the max. dry density (ρ_{max}) is 1.55 g/cm^3. Soil composition and properties are shown in Table 1 whereas the compaction curve is shown in Fig. 1.

2.1 Test specimen

Table 2 Physical properties soil specimens

Property	Dc 65%	Dc 75%	Dc 85%
m (g)	234	264	288
w (%)	15.02	14.95	15.05
ρ_d (g/cm^3)	1.050	1.180	1.300
S_r (%)	27.00	32.00	38.50
e	1.510	1.300	1.050
Initial suction (kPa)	28	29	29

Static compaction was performed in five (05) layers, each 2 cm thick to get homogenous density in the specimen (Rasool *et al.* 2015), by using a static compression machine. A triaxial specimen with height ten (10) cm, diameter 05 cm and water content of 15% was prepared using this method. 15% water content is on the dry side of optimum water content. The specimens in this study are compacted to a degree of compaction (*Dc*) of 65%, 75% and 85% (Chang *et al.* 2011). Specimens prepared with 65% degree of compaction represents the loose soil having a void ratio 1.510, 75% represents a medium dense soil having a void ratio 1.300 and 85% represents a dense soil having a void ratio 1.050. The initial matric suction of soil specimens was measured by putting specimens prepared with 15% water content on a saturated pedestal having a microporous membrane. Fig. 5(a) shows an actual picture of the pedestal with porous stone and a membrane, whereas, the placement of the specimen on the pedestal for the measurement of the initial section is shown in Fig. 5(b) & (c). The initial matric suction of soil specimens prepared with water content 15% and the degree of compaction 65%, 75% & 85% was 28, 29 & 30 kPa respectively. This is compatible with the results of (Rasool and Kuwano 2021, Yang *et al.* 2012) who stated that the compaction energy has less effect on soil suction for the soils with less clay fraction. The specimens prepared with 65% and 75% degree of compaction were normally consolidated specimens with an over-consolidation ratio (*OCR*) equal to 1. Whereas the OCR of specimens prepared with 85% degree of compaction was more than 1, hence they were over-consolidated specimens. The properties of test specimens are presented in Table 2.

2.2 Soil Water Retention Curve (SWRC)

The behavior of unsaturated soils is mainly governed by its soil-water retention curve (*SWRC*) which is the relation between the amount of water in soil pores (in terms of volumetric water content, saturation ratio, gravimetric water content, etc.) and soil matric suction. The soil-water retention behavior is fundamental to a comprehensive understanding of the water flow, deformation processes, and shears strength for unsaturated soils. Many researchers have studied the soil-water retention behavior of unsaturated soils (Gao *et al.* 2018, Gao *et al.* 2021, Konrad and Lebeau 2015, Rasool and Aziz 2020, Zhou *et al.* 2016). SWRC is typically determined using a pressure plate apparatus or tempe pressure cell. Although the current test apparatus has also been used to evaluate the *SWRC* relationship. Several samples with different moisture content were prepared and placed on top of a membrane filter and initial suction

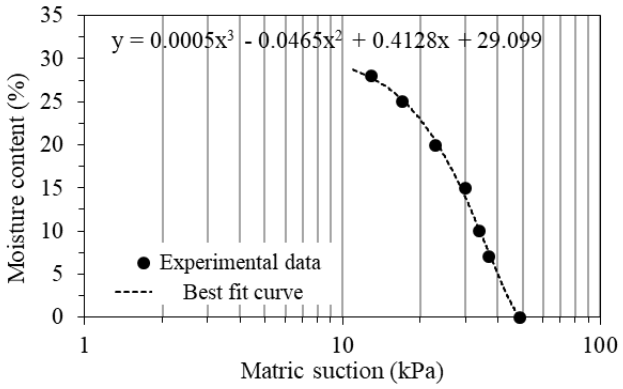

Fig. 2 Soil water characteristic curve of test soil

readings were recorded; Farooq *et al*. (2004) used the same technique to draw SWRC. The SWRC curve in Fig. 2 initially showed a non-linear behavior followed by the linear behavior indicating that the soil suction increases with a decrease in moisture content. It is found that the air-entry suction of the studied soil was around 11 kPa.

3. Test apparatus

The apparatus used was a modern strain-controlled triaxial device appropriate for testing partially saturated soils. The apparatus consists of a double cell, pore air pressure (*PAP*), pore water pressure (*PWP*) & cell pressure transducers. Along with a loading device for applying an axial load, LCDPT for measuring volume change, and an appropriate computer program for monitoring test order and recording experimental data. The volume of the soil sample was determined by a Low Capacity Differential Pressure Transducer (*LCDPT*). The mechanism of measurement of volume change of specimen through LCDPT is that before starting the test, the water level in the inner cell is kept higher than the water level in the outer cell. The water level in the outer cell is kept fixed and taken as a reference. When the specimen contracts the level of water in the inner cell moves downwards and when the soil specimen dilates the water level moves upwards (Rasool *et al.* 2020). The change in water level is recorded by computer software which is then calculated as total volume change of specimen as per relation given in Japanese Geotechnical Society standard (JGS 0527, 2020). The schematic description of the triaxial system used in this research is shown in Fig. 3. A membrane filter and a PTFE (also known as Teflon) layer was used to isolate the routes for the evaluation and monitoring of pore air pressure and pore water pressure. Fig. 4(a) shows the thin membrane with pore size and thickness 0.45 μm & 140 μm respectively. The provided air entry value of the membrane filter was 250 kPa. Fig. 4(b) shows the top cap having pore air pressure

Table 3 Maximum capacities of various devices

CH	Device/Transducers	Maximum Capacity
1	Load Cell	10 kN
2	Axial Displacement	50 mm
3	Cell Pressure	1 MPa
4	Pore Water Pressure	1 MPa
5	Pore Air Pressure	200 kPa
6	External Balance	100 gms

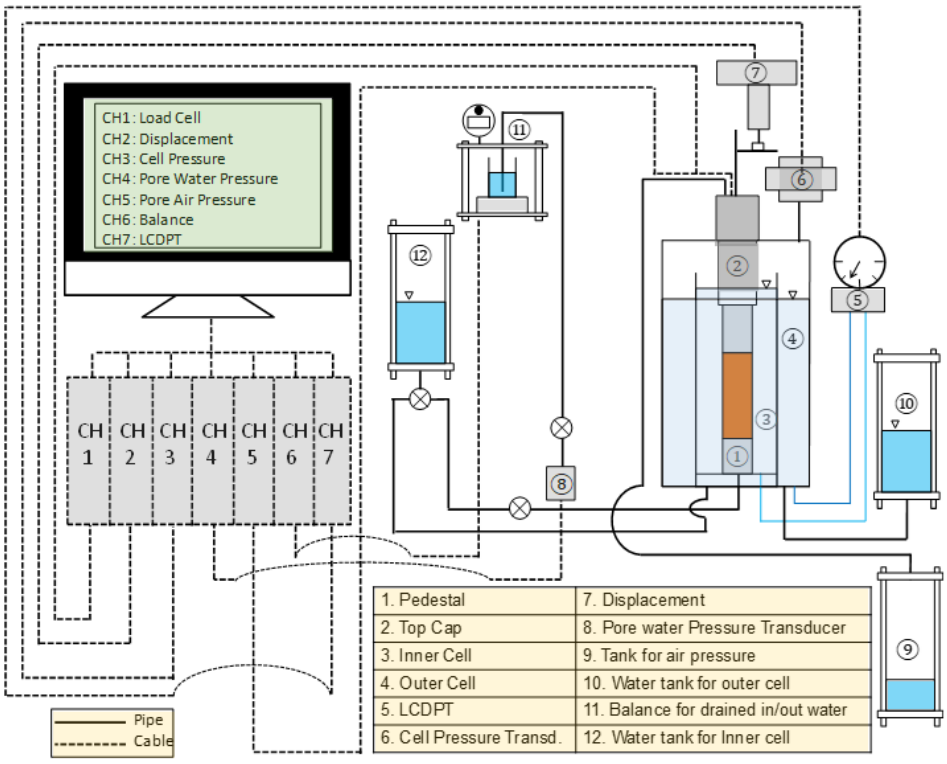

Fig. 3 Schematic illustration of the triaxial apparatus used in the present study

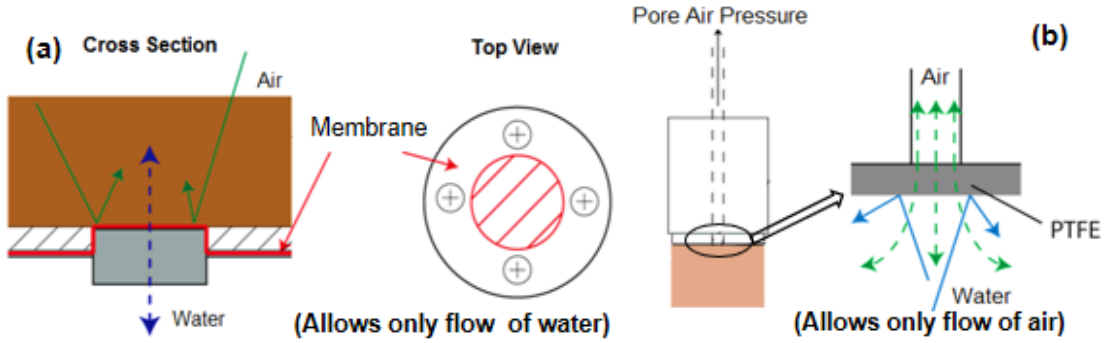

Fig. 4 Schematic representation of (a) Bottom pedestal with the membrane (b) Top Cap with PTFE sheet

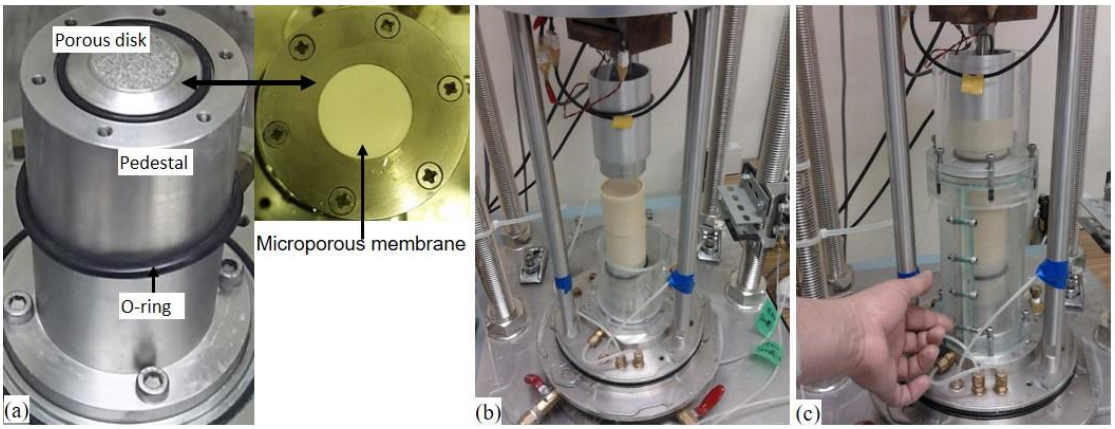

Fig. 5 (a) Actual picture of pedestal with porous stone and membrane, (b) Placement of specimen on the pedestal for the measurement of the initial section, (c) Specimen encased in inner cell

transducer and solenoid valve for controlling drained & undrained air pressure. The PTFE was attached to the bottom of the upper cap to restrict the water flow and control the air pressure. To restrict the airflow, the membrane filter was mounted on a bottom pedestal. In this series, water in the specimen was infiltrated from the bottom pedestal ① connected to beaker and water pressure transducer ⑧ through a water line. The beaker was fitted on a sensitive load cell placed in a cylindrical cell with closed top cap ⑪. The water infiltration rate was regulated by controlling the infiltration pressure applied on top of the cylindrical cell ⑪. A constant infiltration pressure assured an almost uniform injection rate, depending on the level of the infiltration pressure (Farooq *et al*. 2004). Before starting each test, a vacuum pressure of -101.3 kPa was applied to porous disk fitted on a bottom pedestal for removing air from the water line connecting porous disk and pore water pressure transducer. Maximum capacities of the various devices used in the triaxial test apparatus e.g., load cell, axial displacement, PAP, PWP, cell pressure transducers, and external load placed in a beaker are listed in Table 3.

4. Experimental procedure

The flow chart and stress path followed by the specimen during the experimental series is shown in Fig. 6. Initial matric suction of specimens with different compactive efforts was measured and axis translation technique was used to keep pore water pressure, u_w (*PWP*) above atmospheric by increasing pore air, u_a (*PAP*) and cell pressures, σ_3 (Jotisankasa *et al.* 2009, Marinho and Oliveira 2012, Melinda *et al.* 2004, Mirzaii *et al.* 2018, Rasool and Kuwano 2018, Thu *et al.* 2006). Point *A* is the point when the specimen has some value of matric suction. The specimens were then confined at a confining pressure of 60, 80 and 120 kPa for approximately 30 minutes (*AB*). With the use of a microporous membrane, the time for stabilization of pore water pressure was reduced considerably as compared with the boundary with a porous ceramic disk. Point B represents the point after isotropic compression where the soil specimen has a certain value of matric suction and confining stress under zero shear stress. All the tests in this research have been performed in two steps. In Step-1, specimens were sheared in constant water content (*CW*) conditions and monotonic loading was applied. During monotonic loading increase in stress with respect to strain was observed and the specimens were sheared up to 15% axial strain, as defined by the Japanese Geotechnical Society Standard (JGS 0527, 2020). Constant water content method is a type of partially drained test in which PAP is kept drained and controlled, whereas, PWP is kept undrained (Rasool and Aziz 2019). *BC* represents the stress path up to maximum shear stress (q_{max}) in constant water content conditions. Point *C* shows the point when specimens attained the maximum shear stress. The maximum deviatoric stress of soil specimens was obtained by performing a separate series of monotonic loading tests,

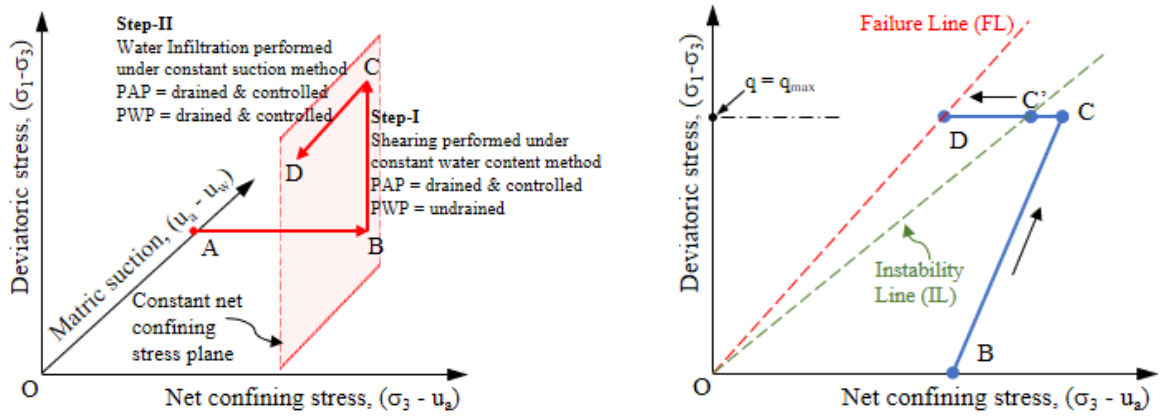

Fig. 6 (a) Stress paths adopted in tests, (b) schematic description of soil behavior during test

Table 4 Stress state of specimens

Degree of Compaction	Loading condition	Test type	Confining pressure (σ_3), kPa	Pore air pressure (u_a), kPa	Pore water pressure (u_w), kPa	Matric suction ($u_a - u_w$), kPa
Dc_65,	Shearing	Constant water content	60	drained & controlled	undrained	varied
Dc_75, Dc_85	Water infiltration	Constant suction	60	drained & controlled	increased in steps	decreased in steps to 0kPa
Dc_65,	Shearing	Constant water content	80	drained & controlled	undrained	varied
Dc_75, Dc_85	Water infiltration	Constant suction	80	drained & controlled	increased in steps	decreased in steps to 0kPa
Dc_65,	Shearing	Constant water content	120	drained & controlled	undrained	varied
Dc_75, Dc_85	Water infiltration	Constant suction	120	drained & controlled	increased in steps	decreased in steps to 0kPa

also explained by the author in (Rasool and Kuwano 2021). The values of maximum deviatoric stress obtained were taken as reference and used in current study. Once the maximum shear stress was achieved, the specimens were moved to the next step. In Step-II, the specimens were sheared in constant suction (*CS*) conditions. The constant suction method is a type of fully drained test in which both PAP and PWP are kept drained and controlled. At the start of Step-II, PWP was decreased and then kept drained and controlled to start water infiltration. Step-II was performed by keeping maximum shear stress constant on the specimens. To perform the test under constant shear stress, the axial loading system of the triaxial test apparatus had the capability of maintaining a constant vertical load for a long time with accuracy. *CD* represents the stress path of water infiltration under constant shear stress. *CD* remains parallel to *OA* and moved towards zero matric suction. The mechanical behavior of studied soil is schematically illustrated in Fig. 6(b). After isotropic compression *B*, the specimen was sheared along stress path *BC*, until maximum shear strength is attained. Then, specimens were subjected to constant shear stress (i.e., C→C'→D) wherein mean effective stress was decreased. At point *C'*, large axial strain started generating without application of any further loading, thus, point *C'* may be termed as the onset of instability and line passing through point *C'* is termed as "Instability Line (IL)". Finally, stress path reached the Failure Line (FL) at point *D*.

5. Experimental results

The state of the soil is one of the key parameters in natural or man-made slopes. Table 4 summarizes the stress states adopted in the current study. A typical nomenclature used in this study to describe the test results is "DcX_cY" where "X" represents specimens prepared with 65%, 75% & 85% degree of compaction (Dc) and "Y" represents the confining pressure of 60, 80 & 120 kPa.

Variation in pore water pressure throughout the test process is shown in Fig. 7. In Step-I, the shearing was performed with constant water content test method, as a result, a minor decrease in pore water pressure i.e., 1-2 kPa was observed in all specimens. Once the specimens reached their maximum shear stress, the specimens were moved to Step-II. In Step-II, the specimens were sheared in constant suction conditions. The PWP was increased by (opening the pore water pressure valve) in steps and kept drained and controlled, as result water started infiltrating into the specimens. Water infiltration in this study was performed by increasing pore water pressure. In some trial tests, it was tried to infiltrate water without increasing/controlling pore water pressure but a very small water volume was infiltrated that was not sufficient to change soil behavior. To

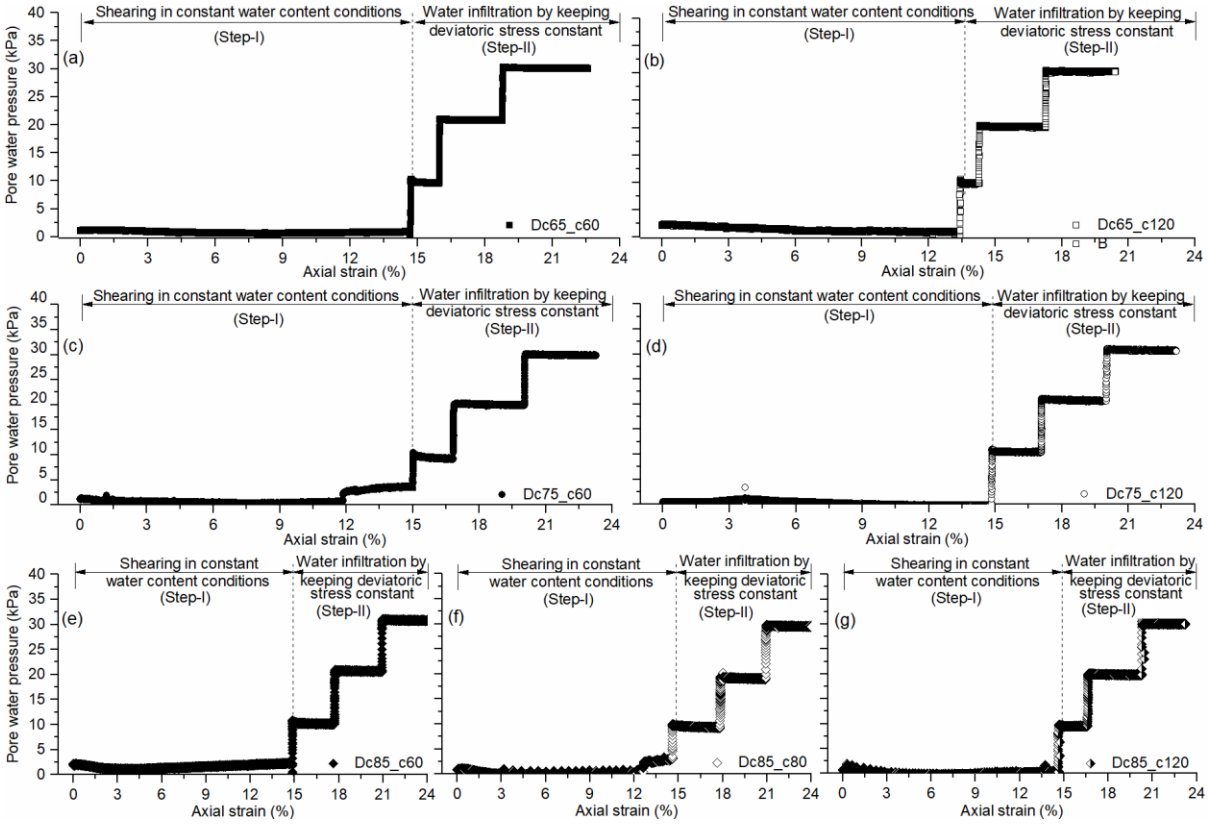

Fig. 7 Change of pore water pressure in specimens (a) Dc65_c60, (b) Dc65_c120, (c) Dc75_c60, (d) Dc75_c120, (e) Dc85_c60, (f) Dc85_c80, (g) Dc85_c120

ensure sufficient water infiltration, one possibility was to shear the soil at a very slow rate, but with the ordinary shear process, it was not possible. Therefore, it was decided to perform water infiltration by controlling the PWP. To avoid an accumulation of water at the base of the specimen, infiltration was performed by increasing the pore water pressure in three (03) steps i.e., from 0 to 10, 10 to 20 and 20 to 30 kPa each with sufficient time of four (04) hours interval (total 12 hrs). In addition, with the use of a microporous membrane, the time for stabilization (Path CD in Fig. 6) of pore water pressure was reduced considerably as compared with the boundary with a porous ceramic disk. Trail tests performed on the specimens also showed that equilibrium was achieved in this time. After that, a very minor change in volume was observed. The increase in PWP in steps can be seen in Figure, which was done by applying infiltration pressure on the cell chamber connected to the bottom pedestal with a valve and pore water pressure transducer through a water line as illustrated in Fig. 3.

Fig. 8 shows the water volume infiltrated in the specimens. In Step-I, during constant water content shearing, the PWP was undrained and measured, therefore, no water infiltration occurred. In Step-II, as soon as the PWP valve was opened, water started infiltrating into the specimens. The Figure shows the step-wise increase in PWP and its effect on increase in the volume of water. The specimens with the degree of compaction 65% and 75% showed compressive behavior during CW shearing, as a result, the void ratio decreased. Hence, the volume of water infiltrated into the specimens decreased with an increase in the degree of compaction. The volume of water infiltrated in specimens Dc65_c60 & Dc65_c120 was 25 cm^3 & 20 cm^3 respectively. In the case of specimens Dc75_c60 & Dc75_c120, volume of water infiltrated into the specimens was 20 cm^3 & 15 cm^3 respectively. The specimens with the degree of compaction 85% showed dilative behavior during CW shearing resulting in an increase in void ratio and increase in the volume of water infiltrated into the specimens.

The volume of water infiltrated in specimens Dc85_c60, Dc85_c80 & Dc85_n120 was 33 cm^3, 25 cm^3 & 16 cm^3 respectively. The test results also showed that increase in confining pressure has a considerable effect on water infiltration. The water infiltration decreased with increase in confining pressure, the same behavior was also reported by (Chen *et al.* 2019, Rasool and Kuwano 2022, 2019).

Fig. 9 shows the variation in the degree of saturation during the shear and water infiltration process. The initial degree of specimens prepared with 65% degree of saturation was 27%. In Step-I, the specimens prepared with 65% degree of compaction showed an increase in the degree of saturation during CW shearing because of compressive behavior. In Step-II, during the water infiltration process, the saturation ratio increased due to increase in the volume of water. 25 cm^3 of infiltrated water raised saturation ratio of specimen Dc65_c60 from 33% to 65% and 20 cm^3 of infiltrated water raised the saturation ratio of specimen Dc65_c120 from 37% to 63%. The initial degree of specimens prepared with 75% degree of saturation was 32%. In Step-I, the specimens prepared with

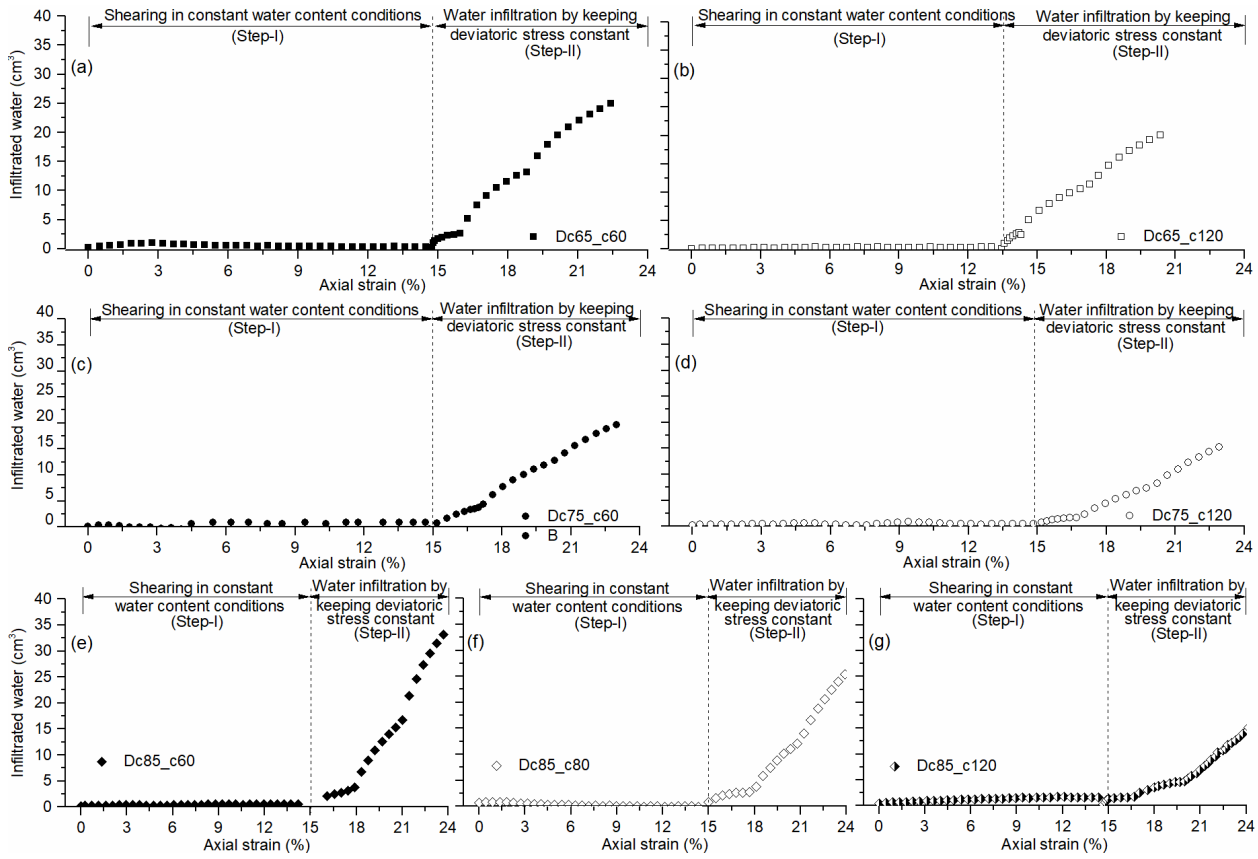

Fig. 8 Volume of water infiltrated in specimens (a) Dc65_c60, (b) Dc65_c120, (c) Dc75_c60, (d) Dc75_c120, (e) Dc85_c60, (f) Dc85_c80, (g) Dc85_c120

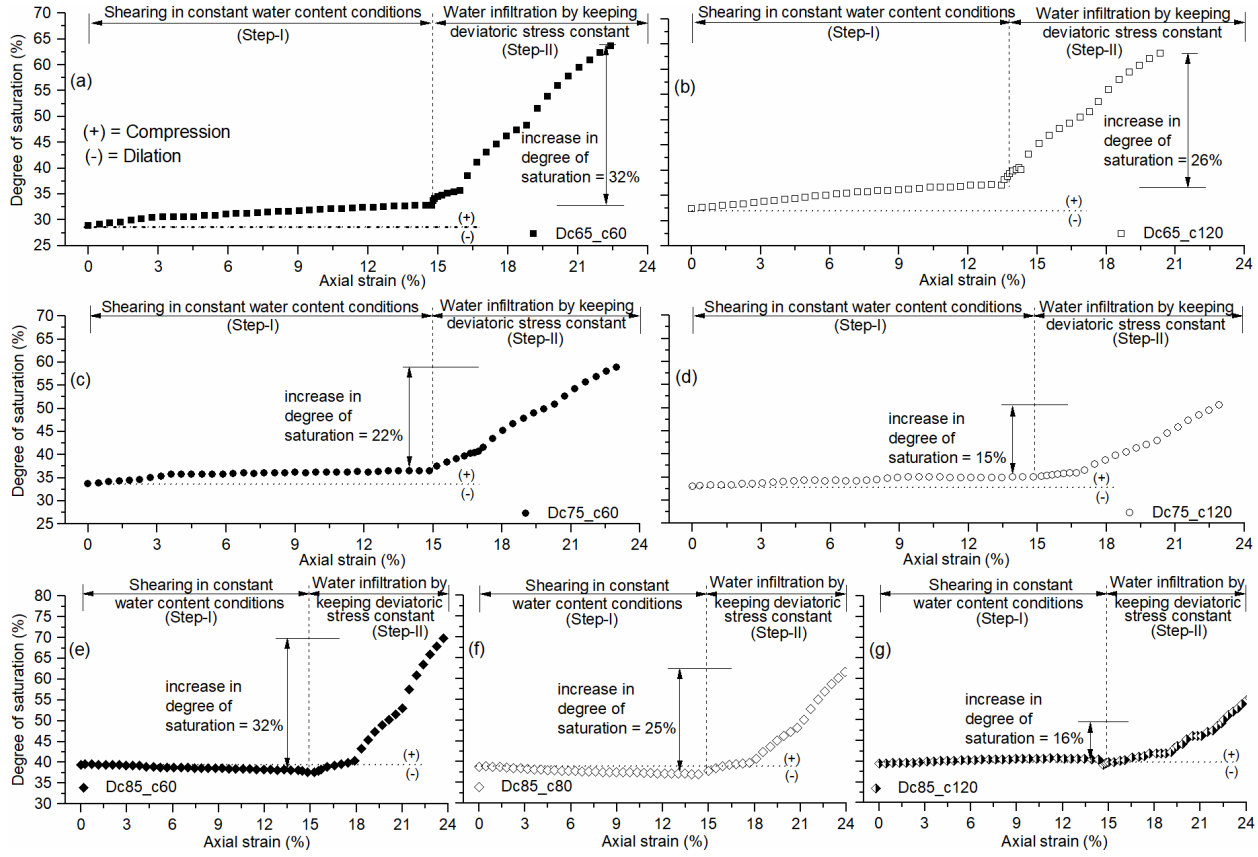

Fig. 9 Variation of degree of saturation in specimens (a) Dc65_c60, (b) Dc65_c120, (c) Dc75_c60, (d) Dc75_c120, (e) Dc85_c60, (f) Dc85_c80, (g) Dc85_c120

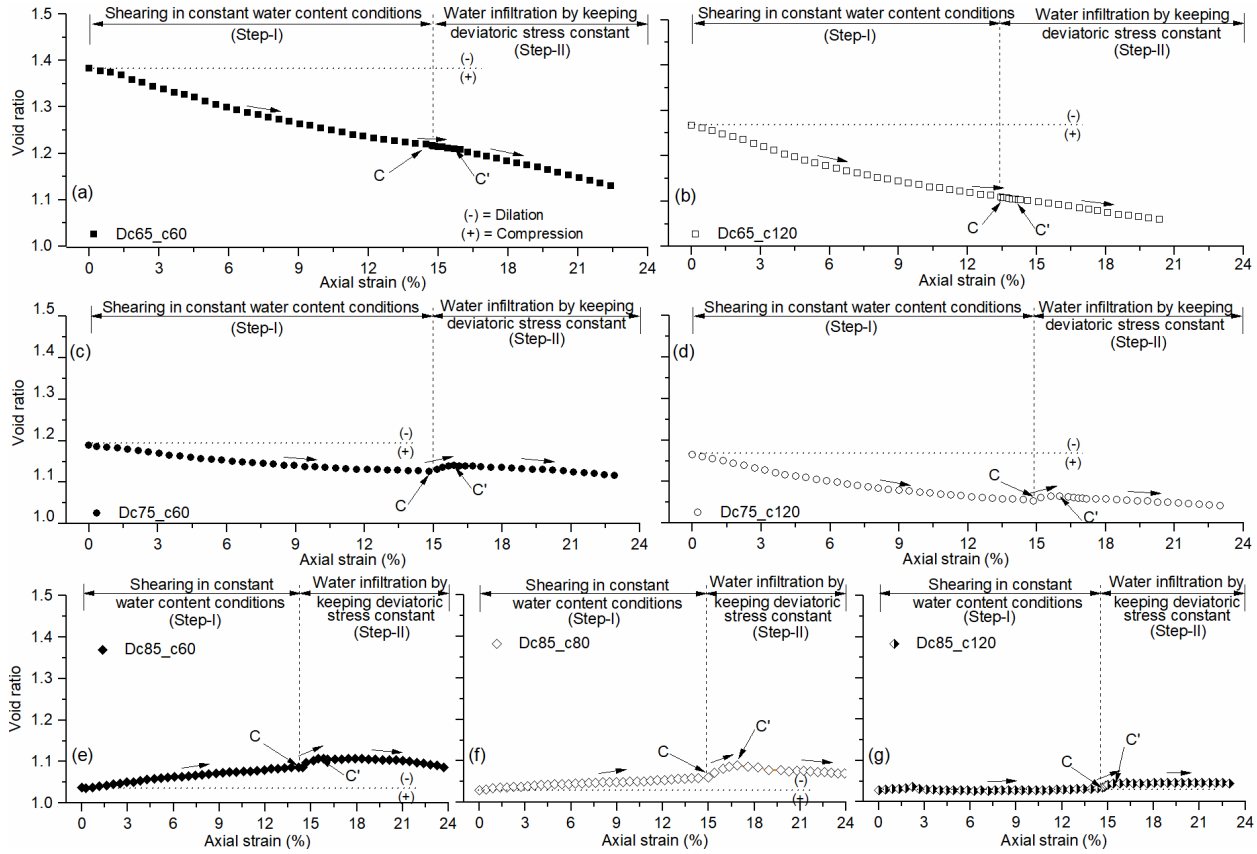

Fig. 10 Deformation behavior of specimens (a) Dc65_c60, (b) Dc65_c120, (c) Dc75_c60, (d) Dc75_c120, (e) Dc85_c60, (f) Dc85_c80, (g) Dc85_c120

75% degree of compaction also showed increase in the degree of saturation due to compressive behavior. In Step-II, during water infiltration process 20 cm^3 of infiltrated water increased degree of saturation of specimen Dc75_c60 from 37% to 59%. Moreover, 15 cm^3 of infiltrated water increased the degree of saturation of specimen Dc75_c120 from 35% to 50%. The initial degree of specimens prepared with 85% degree of saturation was 39%. In Step-I, the specimens prepared with 85% degree of compaction showed decrease in the degree of saturation due to dilative behavior. However, in Step-II, an increase in saturation ratio was noted due to water infiltration. During water infiltration process 33 cm^3 of infiltrated water raised saturation ratio of Dc85_c60 from 38% to 70%, 25 cm^3 of infiltrated water raised saturation ratio of Dc85_c80 from 38% to 63%, and 16 cm^3 of infiltrated water increased the degree of saturation of specimen Dc85_c120 from 40% to 56%.

It can be noted that the maximum increase in the degree of saturation (due to water infiltration) for any specimen was 32% and the maximum degree of saturation was 70%, which was observed for Dc85_c60. Specimen Dc65_c60 also showed 32% increase in the degree of saturation during water infiltration but the maximum degree of saturation was 65%. It is also important here to mention that the purpose of this research was not to achieve 100% degree of saturation but to give adequate equal time intervals for water infiltration so that its behavior on the degree of saturation can be observed. Furthermore, test performed by the Authors (Rasool and Kuwano 2020b, 2022) and other researchers showed that 85% degree of saturation is the maximum degree of saturation of the studied soil. This implies that even at zero suction or at small negative suction, the specimens could not be completely saturated. The incomplete absolute saturation at zero suction can be due to the trapped air in the pores within the specimens and/or in the test system. It was observed that Dc65_60 (specimen with a low degree of compaction and low confining pressure) having compressive behavior showed the same increase in the degree of saturation as of specimen Dc85_80 (specimen with a high degree of compaction and low confining pressure) having dilative behavior. This shows that the degree of compaction has a significant effect on the degree of saturation.

The deformation behavior of specimens in terms of variation in void ratio throughout the test process is presented in Fig. 10. In defining the test results, a decrease in the void ratio is termed as compression of the specimen and an increase in the void ratio is named as dilation of the specimen. In Step-I, the specimens prepared with 65 & 75% degree of compaction showed compressive behavior, whereas, the specimens prepared with 85% degree of compaction showed dilative behavior during CW shearing. This indicates that the deformation behavior of soil is very much dependent on the compactive energies. It can be observed that compression of specimens increased with an increase in confining pressure. Whereas, the dilatation decreased with an increase in confining pressure. After achieving the maximum shear stress, the specimens were

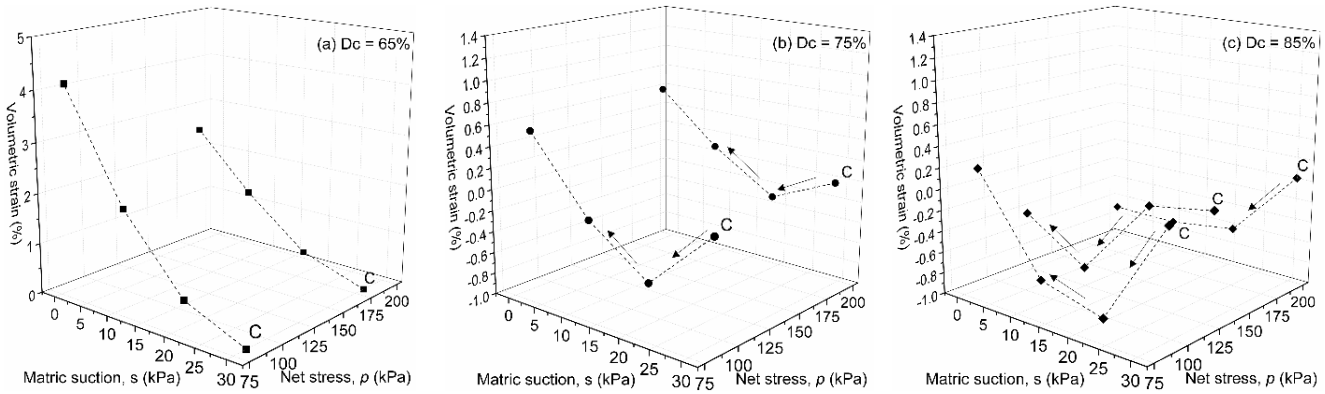

Fig. 11 Three-dimensional plot to explain the deformation behavior of specimens during water infiltration, prepared with degree of compaction (a) 65%, (b) 75%, (c) 85%

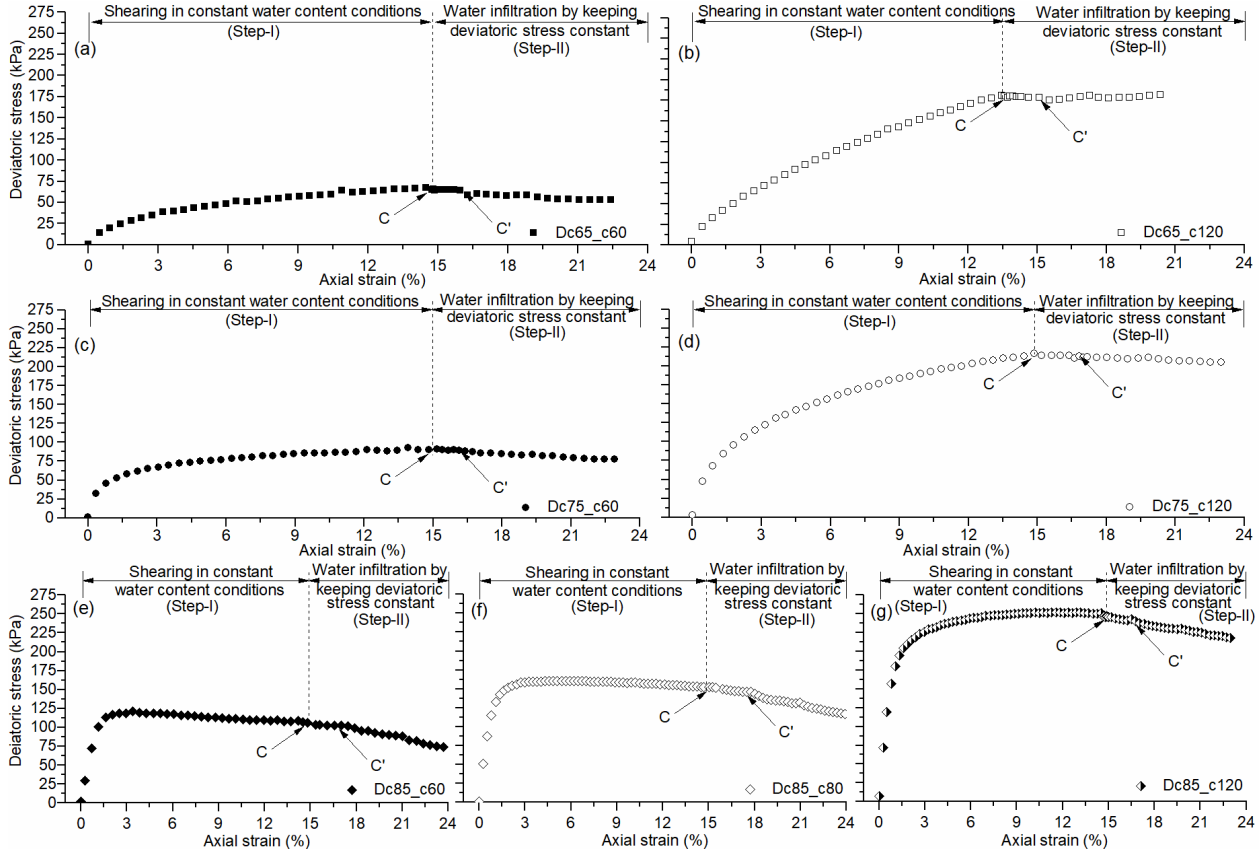

Fig. 12 Stress-strain behavior of specimens (a) Dc65_c60, (b) Dc65_c120, (c) Dc75_c60, (d) Dc75_c120, (e) Dc85_c60, (f) Dc85_c80, (g) Dc85_c120

moved to Step-II. In Step-II, during water infiltration, at Point C', a subsequent reversal i.e., decrease after increase in void ratio was observed in all specimens, except Dc85_120 which exhibited nearly constant trend after increase in void ratio. The subsequent reversal showed the initiation of instability due to the commencement of the water infiltration process.

A three-dimensional plot for each degree of compaction is drawn in Fig. 11 to explain the deformation behavior of specimens during water infiltration. Point C shows the point when water infiltration is started by maintaining constant shear stress. The Figure illustrates that change in volumetric strain due to decreasing suction is small at relatively high matric suctions while the change is more at low matric suctions. In all Figures, as the sample dilates, the volumetric strain starts to increase due to the start of water infiltration (Point C), indicating it as the onset of instability. The specimens prepared with 85% degree of compaction showed small variation in the volumetric strain as compared to specimens prepared with other degree of compactions with decrease in matric suction. The small deformation is due to the dilative behavior of specimens during CW shearing.

Fig. 12 shows the stress-strain relationship. In Step-I, it can be seen that for all considered degree of compactions the shear stress increased with axial strain during CW

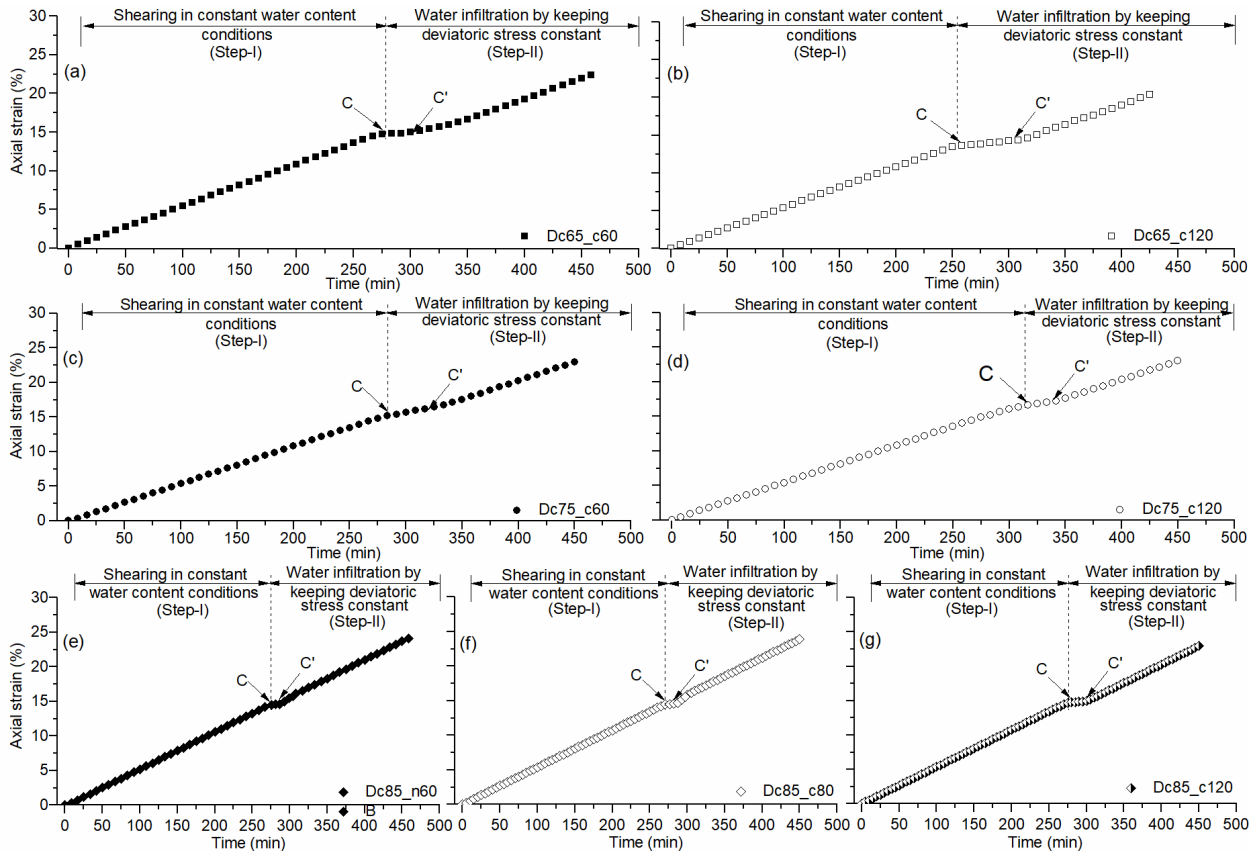

Fig. 13 Development of axial strain in specimens (a) Dc65_c60, (b) Dc65_c120, (c) Dc75_c60, (d) Dc75_c120, (e) Dc85_c60, (f) Dc85_c80, (g) Dc85_c120

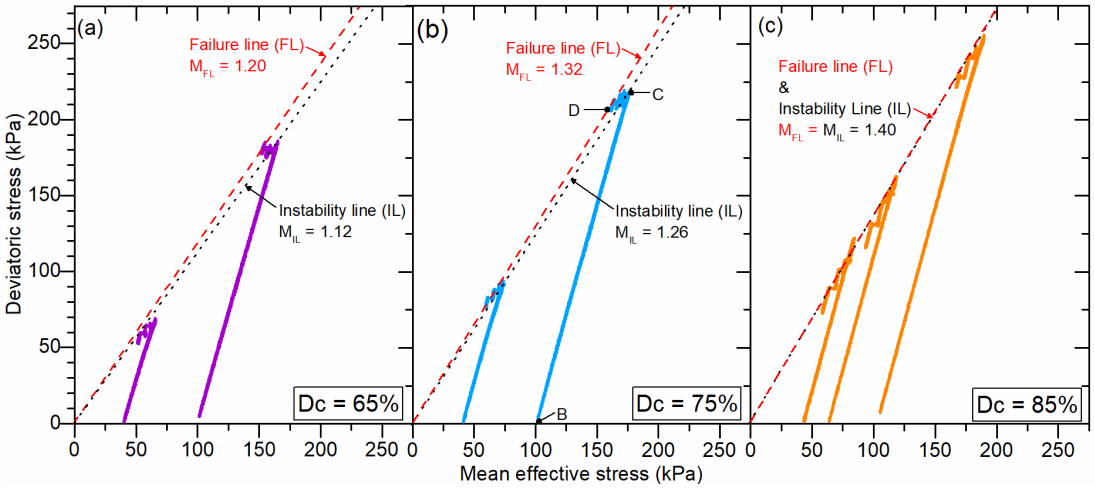

Fig. 14 Instability and failure line

shearing. The shear stress also increased with an increase in confining pressure. The soil specimens prepared with 65% & 75% degree of compaction showed compressive behavior (i.e., decrease in volume) while the specimens prepared with 85% degree of compaction showed dilative behavior (i.e., increase in volume). The difference in soil behavior can also be noticed from stress-strain curves. For the soil specimens that showed dilation, their stress-strain curves are steeper than the ones that showed compression during constant water content shearing, indicating stiff soil behavior. Fig. 13 shows that during CW shearing, development of axial strains is linear with elapsed time up to Point C due to increase in shear stress. Point *C* shows the point when the specimens were moved to Step-II, i.e., water infiltration was performed by maintaining constant shear stress. From Point *C* to *C'*, it can be seen that curve remains almost straight i.e., no much axial strains are produced. However, after Point *C'* large plastic has been developed, that can be seen from the Figure. These plastic strains are developed due to water infiltration without the application of any additional vertical loading. Therefore, point *C'* is considered as the onset of instability. Due to the

development of plastic strain, the shear stress could not remain constant and a decrease in shear stress can be seen in all specimens. However, the amount of decrease in shear stress varied with the degree of compaction, dense soil specimens showed maximum decrease which indicates that the instability has occurred together with the failure in the soil.

5.1 Instability line and failure line

Fig. 14 shows the effective stress paths of the specimens. A plot of the theoretical relationship between two stress parameters is termed as stress path, which is plotted against mean effective stress $p'=(\sigma 1'+2\sigma 3')/3+Sr(ua-uw)$ i.e., a combination of mean net stress and suction stress. As explained earlier, In Step-I, the specimens were sheared in CW conditions along path *BC*. The shear stress increased with mean effective stress and stress path maximum shear stress. As soon as the maximum shear stress was attained, the specimens were moved to Step-II. In Step-II, specimens were sheared in CS conditions keeping the maximum shear stress constant. The pore water pressure valve was opened to increase PWP pressure and decrease matric suction, as a result, stress path moved from point *C* to *D*. During movement of stress point from *C* to *D*, instability occurred somewhere at *C*'. Failure line (*FL*) and instability line (*IL*) for soil specimens with different stress histories are also plotted in Fig. 14. The line obtained by joining the point *C'* on the stress path is the instability line. Whereas, the line obtained by joining the point *D* on the stress path is Failure line. In all tests, failure is said to occur at the point (Point *D*) where the mean effective stress reaches the failure line (*FL*). Whereas various terminologies have been used to define instability line (*IL*) like collapse surface, flow liquefaction surface and yield strength envelop (Sladen *et al*. 1985, Olson and Stark 2003). However, the variations between these terms are minor, and physical concepts behind these terminologies are similar, i.e., a point of yield where large plastic strain starts to develop. It can be observed from Figure that for all considered degree of compactions slopes for both FL (M_{FL}) and IL (M_{IL}) increased with an increase in the degree of compaction, which indicates that the behavior of soil is affected much with variation in stress history. It can also be noted that for loose and medium dense soil specimens compacted with 65% and 75% degree of compaction instability line (*IL*) is located below the failure line (*FL*), which indicates that these soils are vulnerable to pre-failure instability i.e., instability occurs before the effective stress path reaches the failure line. Whereas, the failure line (*FL*) and instability line (*IL*) is unique for the dense soil specimens compacted with 85% degree of compaction, which indicated that the instability has occurred together with failure.

6. Conclusions

In this study, the instability behavior of unsaturated silty soils under different degree of compactions and confining stresses was studied by performing element tests. Understanding the importance, all tests in this study were performed using the modern triaxial test apparatus that has the capability of maintaining constant stress for a long time duration. The following conclusions are drawn from the study:

- Degree of compaction and confining stress has a considerable effect on the behavior of unsaturated soil, loose and medium dense soil shows less water infiltration, whereas, densely compacted soil shows more water infiltration during the water infiltration process.
- Water infiltration is found to be the main cause of instability in soil, it changed the soil behavior from compression to dilation and produced large plastic deformation without having to have any additional vertical loading.
- Experimental results indicated that loose and medium dense soils are susceptible to pre-failure instability i.e., instability can occur before the effective stress path reaches the failure line (*FL*).
- For dense soils the failure line (*FL*) and instability line (*IL*) is found unique, indicating instability occurred together with the failure.

Acknowledgments

The Saitama University Japan and Japanese Ministry of Education, Culture, Sports, Science and Technology (MEXT) is gratefully acknowledged for research facilities and financial assistance

References

Andrade, J.E., Ramos, A.M. and Lizcano, A. (2013), "Criterion for flow liquefaction instability", *Acta Geotechnica*, **8**, 525-535. https://doi.org/10.1007/s11440-013-0223-x.

ASTM D2487 (2011), Standard Practice for Classification of Soils for Engineering Purposes (Unified Soil Classification System), ASTM International.

Chang, D.S., Zhang, L.M., Xu, Y. and Huang, R.Q. (2011), "Field testing of erodibility of two landslide dams triggered by the 12 May Wenchuan earthquake", *Landslid.*, **8**(3), 321-332. https://doi.org/10.1007/s10346-011-0256-x.

Chen, M., Zhou, Z., Sleep, B., Kuang, X., Mingwei, L. and Shi, A. (2019), "Experimental study of water infiltration in unsaturated horizontal sand columns under various air confinement conditions", *Geofluid.*, **2019**, 4270358. https://doi.org/10.1155/2019/4270358.

Chen, P., Wei, C., Liu, J. and Ma, T. (2013), "Strength theory model of unsaturated soils with suction stress concept", *J. Appl. Math*., **2013**, Article ID 756854. https://doi.org/10.1155/2013/756854.

Chu, J., Leong, W.K., Loke, W.L. and Wanatowski, D. (2011), "Instability of loose sand under drained conditions", *J. Geotech. Geoenviron. Eng.*, **138**, 207-216. https://doi.org/10.1061/(ASCE)GT.1943-5606.0000574.

Chu, J., Leroueil, S. and Leong, W.K. (2003), "Unstable behaviour of sand and its implication for slope instability", *Can. Geotech. J.*, **40**(5), 873-885. https://doi.org/10.1139/t03-039.

Chu, J. and Wanatowski, D. (2009), "Effect of loading mode on strain softening and instability behavior of sand in plane-strain

tests", *J. Geotech. Geoenviron. Eng.*, **135**(1), 108-120. https://doi.org/10.1061/(ASCE)1090-0241(2009)135:1(108).

Consoli, N.C., Da Silva Lopes, L., Consoli, B.S., Festugato, L., Di Sante, M., Fratalocchi, E. and Mazzieri, F. (2015), "Mohr-coulomb failure envelopes of lime-treated soils", *Geotechnique*, **65**(10), 866-868. https://doi.org/10.1680/jgeot.15.D.001.

Desai, C.S., Pradhan, S.K. and David, C. (2005), "Cyclic testing and constitutive modeling of saturated sand-concrete interfaces using the disturbed state concept", *Int. J. Geomech.*, **5**(4), 286-294. https://doi.org/10.1061/(ASCE)1532-3641(2005)5:4(286).

Dong, Q., Xu, C., Cai, Y., Juang, H., Wang, J., Yang, Z. and Gu, C. (2016), "Drained instability in loose granular material", *Int. J. Geomech.*, **16**(2), 04015043. https://doi.org/10.1061/(ASCE)GM.1943-5622.0000524.

Farooq, K., Rolando, O. and Ikuo, T. (2004), "Response of unsaturated sandy soils under constant shear stress drained condition", *Soil. Found.*, **44**(2), 1-13. http://doi.org/10.3208/sandf.44.2_1.

Fredlund, D.G., Rahardjo, H. and Fredlund, M.D. (2012), *Unsaturated Soil Mechanics in Engineering Practice*, John Wiley & Sons, Inc.

Gao, Y., Sun, D., Zhou, A. and Li, J. (2018), "Effect of stress state on soil-water retention and its application on the strength prediction", *Géotechnique Lett.*, **8**(4), 324-329. https://doi.org/10.1680/jgele.18.00159.

Gao, Y., Li, Z., Sun, D. and Yu, H. (2021), "A simple method for predicting the hydraulic properties of unsaturated soils with different void ratios", *Soil Tillage Res.*, **209**, 104913. https://doi.org/10.1016/j.still.2020.104913.

Gui, M.W. and Wu, Y.M. (2014), "Failure of soil under water infiltration condition", *Eng. Geol.*, **181**, 124-141. https://doi.org/10.1016/j.enggeo.2014.07.005.

JGS 0527 (2020), Method for Triaxial Compression Test on Unsaturated Soils, Japanese Geotechnical Society Standard, 1-12.

Jotisankasa, A., Coop, M. and Ridley, A. (2009), "The mechanical behaviour of an unsaturated compacted silty clay", *Geotechnique*, **59**(5), 415-428. https://doi.org/10.1680/geot.2007.00060.

Konrad, J.M. and Lebeau, M. (2015), "Capillary-based effective stress formulation for predicting shear strength of unsaturated soils", *Can. Geotech. J.*, **52**(12), 2067-2076. https://doi.org/10.1139/cgj-2014-0300.

Labuz, J.F. and Zang, A. (2012), "Mohr-Coulomb failure criterion", *Rock Mech. Rock Eng.*, **45**(6), 975-979. https://doi.org/10.1007/s00603-012-0281-7.

Lashkari, A. (2016), "Prediction of flow liquefaction instability of clean and silty sands", *Acta Geotechnica*, **11**, 987-1014. https://doi.org/10.1007/s11440-015-0413-9.

Leong, W., Chu, J. and Teh, C. (2000), "Liquefaction and instability of a granular fill material", *Geotech. Test. J.*, **23**(2), 178-192. https://doi.org/10.1520/GTJ11042J.

Liu, J., Yang, C., Gan, J., Liu, Y., Wei, L. and Xie, Q. (2017), "Stability analysis of road embankment slope subjected to rainfall considering runoff-unsaturated seepage and unsaturated fluid-solid coupling", *Int. J. Civil Eng.*, **15**(6), 865-876. https://doi.org/10.1007/s40999-017-0194-7.

Marinho, F.A.M. and Oliveira, O.M. (2012), "Unconfined shear strength of compacted unsaturated plastic soils", *Proc. Inst. Civil Eng.: Geotech. Eng.*, **165**(2), 97-106. https://doi.org/10.1680/geng10.00027.

Meilani, I., Rahardjo, H. and Leong, E.C. (2005), "Pore-water pressure and water volume change of an unsaturated soil under infiltration conditions", *Can. Geotech. J.*, **42**(6), 1509-1531. https://doi.org/10.1139/t05-066.

Melinda, F., Rahardjo, H., Han, K.K. and Leong, E.C. (2004), "Shear strength of compacted soil under infiltration condition", *J. Geotech. Geoenviron. Eng.*, **130**(8), 807-817. https://doi.org/10.1061/(ASCE)1090-0241(2004)130:8(807).

Mirzaii, A., Yasrobi, S.S. and Hefzi, E. (2018), "Critical state behaviour of an unsaturated clayey sand along constant water content direct shear and triaxial loading conditions", *Int. J. Geotech. Eng.*, **14**(3), 286-294. https://doi.org/10.1080/19386362.2018.1438151.

Monkul, M., Yamamuro, J. and Lade, P. (2011), "Failure, instability, and the second work increment in loose silty sand", *Can. Geotech. J.*, **48**, 943-955. https://doi.org/10.1139/t11-013.

Mróz, Z., Boukpeti, N. and Drescher, A. (2003), "Constitutive model for static liquefaction", *Int. J. Geomech.*, **3**(2), 133-144. https://doi.org/10.1061/(ASCE)1532-3641(2003)3:2(133).

Qi, S., Vanapalli, S.K., Yang, X., Zhou, J. and Lu, G. (2019), "Stability analysis of an unsaturated expansive soil slope subjected to rainfall infiltration", *Geomech. Eng.*, **19**(1), 1-9. https://doi.org/10.12989/gae.2019.19.1.001.

Rahardjo, H., Kim, Y. and Satyanaga, A. (2019), "Role of unsaturated soil mechanics in geotechnical engineering", *Int. J. Geo-Eng.*, **10**(1), 1-23. https://doi.org/10.1186/s40703-019-0104-8.

Rahman, M.M., Baki, M.A. and Lo, S.R. (2014), "Prediction of undrained monotonic and cyclic liquefaction behavior of sand with fines based on the equivalent granular state parameter", *Int. J. Geomech.*, **14**(2), 254-266. https://doi.org/10.1061/(ASCE)GM.1943-5622.0000316.

Rasool, A.M. and Aziz, M. (2019), "Shear infiltration and constant water content tests on unsaturated soils", *Geomech. Eng.*, **19**(5), 435-445. https://doi.org/10.12989/gae.2019.19.5.435.

Rasool, A.M. and Aziz, M. (2020), "Advanced triaxial tests on partially saturated soils under unconfined conditions", *Int. J. Civil Eng.*, **18**(10), 1139-1156. https://doi.org/10.1007/s40999-020-00530-7.

Rasool, A.M. and Kuwano, J. (2018), "Influence of matric suction on instability of unsaturated silty soil in unconfined conditions", *Int. J. GEOMATE*, **14**(42), 1-7. https://doi.org/10.21660/2018.42.7115.

Rasool, A.M. and Kuwano, J. (2020a), "Shearing infiltration tests to study mechanical behavior and failure mechanism of shallow slopes", *Iran. J. Sci. Technol.-Trans. Civil Eng.*, **45**(2), 1089-1098. https://doi.org/10.1007/s40996-020-00403-y.

Rasool, A.M. and Kuwano, J. (2020b), "Effect of constant loading on unsaturated soil under water infiltration conditions", *Geomech. Eng.*, **20**(3), 221-232. https://doi.org/10.12989/gae.2020.20.3.221.

Rasool, A.M. and Kuwano, J. (2020c), "Effect of constant loading on unsaturated soil under water infiltration conditions", *Geomech. Eng.*, **20**(3), 221-232. https://doi.org/10.12989/GAE.2020.20.3.221.

Rasool, A.M. and Kuwano, J. (2021), "Instability of unsaturated soils under constant deviatoric stress in drained conditions", *Iran. J. Sci. Technol.-Tran. Civil Eng*, **46**(1), 419-434. https://doi.org/10.1007/s40996-021-00582-2.

Rasool, A.M. and Kuwano, J. (2022), "Effect of wetting stress paths on mechanical behavior and instability of unsaturated soil in stress state space", *Eur. J. Environ. Civil Eng.*, 1-20. https://doi.org/10.1080/19648189.2022.2025909.

Rasool, A.M. and Kuwano, J. (2019), "Effect of water infiltration on the mechanical behaviour of unsaturated soil", *E3S Web Conf.*, **92**, 1-6. https://doi.org/10.1051/e3sconf/20199207002.

Rasool, A.M., Kuwano, J. and Tachibana, S. (2015), "Behavior of compacted unsaturated soil in isotropic compression, cyclic and monotonic shear loading sequences in undrained condition", *Deformation Characteristics of Geomaterials*, January, 267-274. https://doi.org/10.3233/978-1-61499-601-9-267.

Rasool, A.M., Kuwano, J. and Tachibana, S. (2020), "Experimental Study on the response of unsaturated silt due to

change in drainage conditions during the triaxial test process", *Geotech. Geolog. Eng.*, **38**(2), 1707-1719. https://doi.org/10.1007/s10706-019-01125-3.

Song, Y.S. and Hong, S. (2020), "Infiltration characteristics and hydraulic conductivity of weathered unsaturated soils", *Geomech. Eng.*, **22**(2), 153-163. https://doi.org/10.12989/gae.2020.22.2.153.

Sun, W.C. (2013), "A unified method to predict diffuse and localized instabilities in sands", *Geomech. Geoeng.*, **8**(2), 65-75. https://doi.org/10.1080/17486025.2012.695403.

Thu, T.M., Rahardjo, H. and Leong, E.C. (2006), "Shear Strength and Pore-water pressure characteristics during constant water content triaxial tests", *J. Geotech. Geoenviron. Eng.*, **132**(3), 411-419. https://doi.org/10.1061/(asce)1090-0241(2006)132:3(411).

Yang, S.R., Lin, H.D. and Huang, W.H. (2012), "Variation of initial soil suction with compaction conditions for clayey soils", *J. Mech.*, **28**(3), 431-437. https://doi.org/10.1017/jmech.2012.52.

Zhao, H.F. and Zhang, L.M. (2014), "Instability of saturated and unsaturated coarse granular soils", *J. Geotech. Geoenviron. Eng.*, **140**(1), 25-35. https://doi.org/10.1061/(ASCE)GT.1943-5606.0000976.

Zhou, A., Huang, R. and Sheng, D. (2016), "Capillary water retention curve and shear strength of unsaturated soils", *Can. Geotech. J.*, **53**(6), 974-987. https://doi.org/10.1139/cgj-2015-0322.

CC